Available online at www.sciencedirect.com
ScienceDirect
Journal of Sound and Vibration 317 (2008) 67–90
JOURNAL OF SOUND AND VIBRATION
www.elsevier.com/locate/jsvi

Vibration control by recursive time-delayed acceleration feedback

S. Chatterjee

Department of Mechanical Engineering, Bengal Engineering and Science University, Shibpur, P.O. Botanic Garden, Howrah 711 103, West Bengal, India

Received 26 November 2007; received in revised form 10 March 2008; accepted 17 March 2008
Handling Editor: J. Lam
Available online 20 May 2008

Abstract

This paper presents a theoretical basis of time-delayed acceleration feedback control of linear and nonlinear vibrations of mechanical oscillators. The control signal is synthesized by an infinite, weighted sum of the acceleration of the vibrating system measured at equal time intervals in the past. The proposed method is shown to have controlled linear resonant vibrations, low-frequency non-resonant vibrations, primary and 1/3 subharmonic resonances of a forced Duffing oscillator. The concept of an equivalent damping and natural frequency of the system is also introduced. It is shown that a large amount of damping can be produced by appropriately selecting the control parameters. For some combinations of the control parameters, the effective damping factor of the system is shown to be inversely related to the time-delay in the small delay limit. Selection of the optimum control parameters for controlling the forced and free vibrations is discussed. It is shown that forced vibration is best controlled by unity recursive gain and smaller values of the time-delay parameter. However, the transient response can be optimally controlled by suitably selecting the time delay depending upon the gain. The delay values for the optimal forced response may be different from that required for the optimum transient response. When both are important, a suboptimal choice of the delay parameters with unity recursive gain is recommended.

1. Introduction

Controlling resonant vibrations of flexible machine components and structural members has always been an important area of research for engineers. Various passive and active methods for controlling resonant vibrations have been proposed and implemented in practice. Though active vibration control is superior to passive control techniques, presence of unavoidable time delays in the feedback circuit seriously limits the performance of an active control system by destabilizing it at high control gains. Engineers [1] have attempted to design the system so as to reduce or eliminate the effect of time delays on the performance and stability of active vibration control systems. However, these techniques work only for time-delays smaller compared to the natural time period of vibration of the system.

The last two decades or so have witnessed a new thread of research on active vibration control that utilizes deliberate time-delays in the measured state of the system. A significant number of theoretical and

E-mail address: shy@mech.becs.ac.in

0022-460X/$ - see front matter © 2008 Elsevier Ltd. All rights reserved.
doi:10.1016/j.jsv.2008.03.020

experimental studies have amply demonstrated the efficacy of this class of control technique, which goes by the name of '*time-delayed feedback control*' in literature. Time-delayed feedback control has been successfully used to control vibrations and stabilities of various linear and nonlinear systems. A comprehensive survey of the recent research on the field is available in Ref. [2]. Olgac et al. [3,4] have developed a new class of active vibration absorber based on linear state feedback with a time-delay, which they have termed as the *delayed resonator*. Udwadia et al. [5–10] have explored the application of time-delayed velocity feedback for controlling the vibrations of structural systems under seismic loading. Several researchers have considered time-delayed feedback control of parametric vibrations, nonlinear resonances and self-excited oscillations of flexible mechanical systems. Hu et al. [11] have reported time-delayed state feedback control of the primary and 1/3 subharmonic resonances of a forced Duffing oscillator. Maccari [12] have studied the primary resonance of a cantilever beam under the time-delayed feedback control. Vibration control of self-excited systems has been studied by Maccari [13–14] and Atay [15]. Chatterjee [16] have discussed time-delayed feedback control of various friction-induced instabilities. Time-delayed feedback control has also been successfully used in reducing the sway of container cranes [17].

Though time-delayed feedback control has been proved to be useful in controlling linear and nonlinear vibrations of various systems, all of the previous studies (to the best of the author's knowledge and information) consider only full or partial state feedback (i.e. displacement and velocity feedback). Because it is difficult to find a suitable inertial frame of reference, direct measurements of displacement and velocity at an arbitrary location are mostly impractical in real-life situations. Alternatively, accelerometers provide an inexpensive and reliable means of measuring accelerations of vibrating components. Moreover, acceleration feedback renders the control non-invasive. Therefore, vibration control strategies based on acceleration feedback offer a practicable means of active vibration control. Though several researchers have already explored this alternative [18–19], more studies are required. Acceleration feedback control principally works by shifting the natural frequency of the vibrating component to a safer value. Ordinary acceleration feedback does not influence the damping properties, whereas time-delayed acceleration feedback can influence the effective damping of the vibrating body.

In this paper, the theoretical basis of a vibration control strategy based on the time-delayed acceleration feedback is presented. The control signal, in the proposed strategy, is determined by an infinite, weighted sum of the acceleration of the vibrating system measured at equally spaced time intervals in the past. The basic idea is adapted from the concept of *Extended Time-delay Auto Synchronization* (ETDAS) control strategy originally proposed by Socolar et al. [20] for stabilizing the unstable periodic orbits embedded in a chaotic attractor. However, the full potential of this class of control strategy in mitigating vibrations of flexible mechanical and structural components are not yet explored. Instead of using delayed difference of the measured states of the system for determining the control signal, as is conventionally done in ETADS, here delayed acceleration determines the control signal. Because the control signal is recursively determined by the weighted sum of the time-delayed acceleration and the time-delayed control signal, the proposed strategy is pertinently called hereafter as the *Recursive Time-delayed Acceleration Feedback Control*. The proposed method is first employed to control the vibration of a single-degree-of-freedom undamped linear mechanical oscillator. The efficacy of the proposed method for controlling the primary and the 1/3 subharmonic resonances of a forced Duffing oscillator is also discussed.

2. Controlling linear vibration

2.1. Mathematical model

The non-dimensional equation of motion of a single-degree-of-freedom undamped oscillator with the proposed control is governed by the following delay differential equation:

$$\ddot{x} + x = f(t) + k_c u, \tag{1}$$

where u is the control signal, k_c the control gain and $f(t)$ the external excitation. Here, the time t is non-dimensionalized with respect to the natural time period of the oscillator.

The control signal u is determined by the infinite weighted sum of the acceleration of the system measured at equal time intervals τ in the past and is mathematically expressed as

$$u = \sum_{k=1}^{\infty} R^{k-1} \ddot{x}(t - k\tau), \tag{2}$$

where R is a real parameter and τ denotes the time-delay parameter non-dimensionalized with respect to the natural time period of oscillation of the system.

Alternatively, the control signal u can be written in the recursive form of as

$$u = \ddot{x}(t - \tau) + Ru(t - \tau). \tag{3}$$

The recursive parameter R generally varies from 0 to 1. It is noteworthy that the case $R = 0$ corresponds to an ordinary time-delayed acceleration feedback. Ordinarily in the discussions to follow, R is less than unity. However, $R = 1$ is also an interesting case which calls for a special attention and hence discussed separately.

The transfer function of the linear system governed by Eqs. (1) and (3) is expressed as

$$G(s) = \frac{X(s)}{F(s)} = \frac{1 - Re^{-s\tau}}{(s^2 + 1)(1 - Re^{-s\tau}) - k_c s^2 e^{-s\tau}}. \tag{4}$$

It should be noted that for $k_c = R = 0$, Eq. (4) reduces to the transfer function of the uncontrolled system.

2.2. Stability analysis

The stability of the trivial equilibrium of the system is ascertained by the roots of the characteristics equation given below:

$$(s^2 + 1) - (k_c s^2 + Rs^2 + R)e^{-s\tau} = 0. \tag{5}$$

Substituting $s = j\omega$ into Eq (5) and separating the imaginary and real parts, yields

$$(1 - \omega^2) - R(1 - \omega^2)\cos\,\omega\tau + k_c\omega^2\,\cos\,\omega\tau = 0, \tag{6a}$$

$$R(1 - \omega^2)\sin\,\omega\tau - k_c\omega^2\,\sin\,\omega\tau = 0. \tag{6b}$$

Because $R(1-\omega^2)-k_c\omega^2$ can be zero only for$\omega = \sqrt{(R/R + k_c)}$, Eq. (6b) leads to

$$\sin\,\omega\tau = 0. \tag{7}$$

The general solution of Eq. (7) is

$$\omega\tau = n\pi, \quad \forall n = 0, 1, 2, \ldots, \infty \tag{8}$$

Substituting Eq. (8) into Eq. (6a), yields the following equation for the critical stability lines:

$$\tau^2 - n^2\pi^2 - (-1)^n\{R\tau^2 - (R + k_c)n^2\pi^2\} = 0. \tag{9}$$

As the uncontrolled system is marginally stable, $k_c = 0$ is also a critical stability line.

Finally, the stable regions in the k_c vs.τ plane are obtained from the sign of the root tendency defined below and listed in Table 1. In the stable regions, the total number of unstable roots should be zero:

$$\Re(\omega_c, \tau_c) = \mathrm{sgn}\left[\mathrm{Re}\left(\left.\frac{ds}{d\tau}\right|_{j\omega_c,\tau_c}\right)\right]. \tag{10}$$

Table 1

$\Re$	Increase in the number of stable roots	Increase in the number of unstable roots
+1		2
−1	2	

Fig. 1 depicts the regions of stability in the k_c vs.τ plane for different values of R. Because the stability region in the lower range of delays is of practical importance, this region is henceforth called as the *primary stability zone*. In the subsequent numerical explorations, parameter values are chosen from the primary stability zone. The negative sign of the control gain in the primary stability zone establishes the fact that the control system is stable under the negative feedback control. From Fig. 1, it is observed that the primary stability zone widens with the increasing value of R. Higher values of R apparently admits using higher values of the control gain. Benefits of using higher values of the control gain will be discussed elsewhere.

It may be noted that for $R = 1$, the characteristics equation (Eq. (5)) has a root at $s = 0$. Thus, the origin of the complex plane is a pole of the system. This appears to be a marginally stable case. However, it is evident from Eq. (5) that the controlled system also has infinite number of closed-loop zeros computed as

$$z_n = \frac{1}{\tau}\ln(R) + j\frac{2n\pi}{\tau} \quad \text{for } n = 0, 1, 2, \ldots, \infty \tag{11}$$

From Eq. (11), it is observed that when $R = 1$, there is a zero at the origin. This closed-loop zero nullifies the effect of the pole at the origin. Consequently, the stability of the trivial equilibrium is determined by the other poles of the system. The primary stability region for $R = 1$ is shown in Fig. 2.

2.3. Frequency-response analysis

Case I: $R<1$. The frequency-response function of the closed-loop system is expressed as

$$\left|G(j\omega)\right| = \frac{\sqrt{[1 - R\cos(\omega\tau)]^2 + [R\sin\omega\tau]^2}}{\sqrt{[1 - \omega^2 - (R - R\omega^2 - k_c\omega^2)\cos\omega\tau]^2 + [(R - R\omega^2 - k_c\omega^2)\sin\omega\tau]^2}}. \tag{12}$$

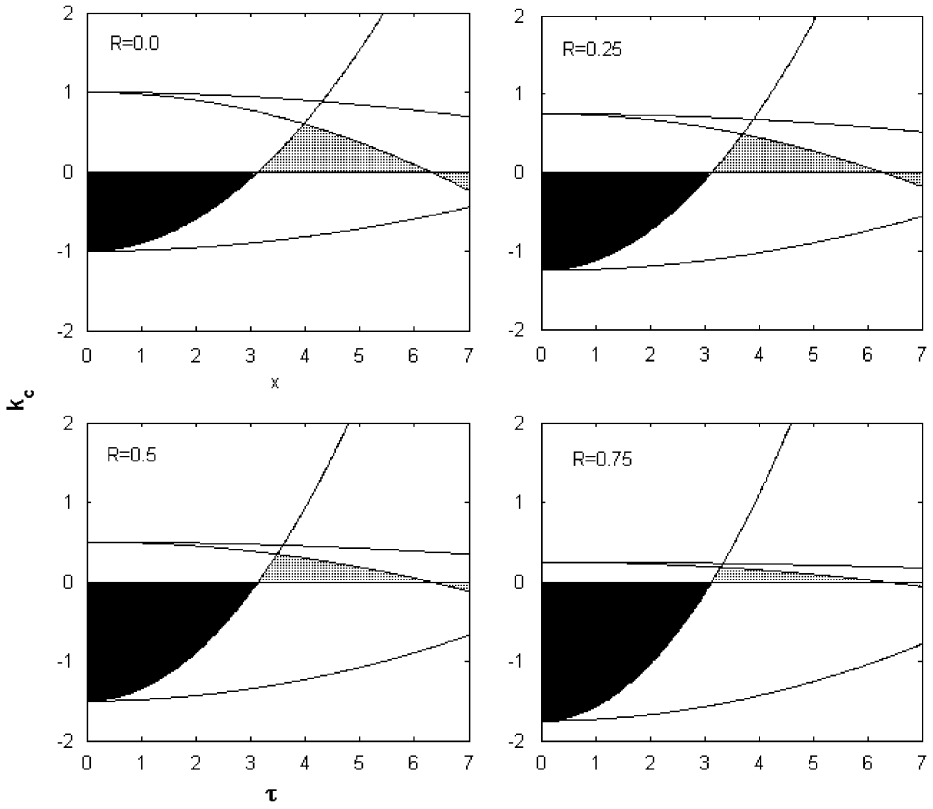

Fig. 1. Stability regions for different values of R (<1). Shaded regions are stable. Black regions are *primary stability zones*. Solid lines represent the critical stability lines for different n on which some of the characteristic roots are purely imaginary.

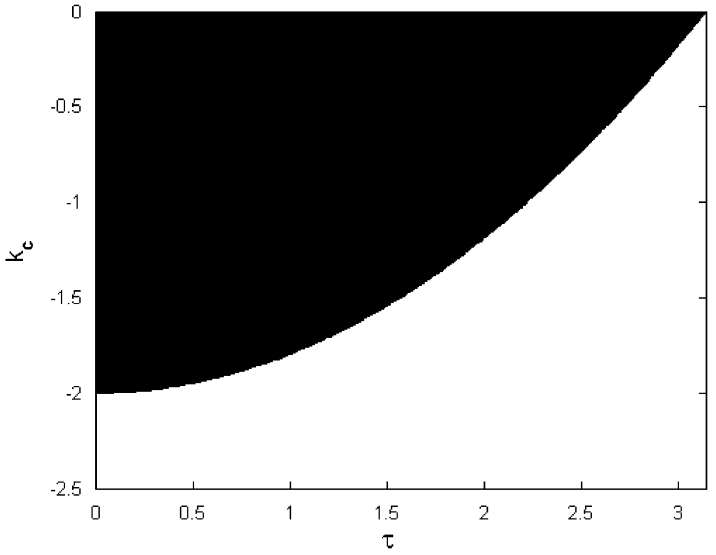

Fig. 2. Primary stability zone for $R = 1$. Black shaded region is stable.

Typical frequency-response plots for different combinations of the parameter values are illustrated in Figs. 3(a) and (b). The important observations made from these plots are listed below:

a. Frequency-response characteristics are apparently more damped (reduced peak) for higher values of R and k_c.
b. Frequency-response plots for different delay values, with the other parameters remaining fixed, pass through a common point. This point is henceforth called the crossing point (CP) and the corresponding frequency is called the *crossing frequency*.
c. With the increasing value of the time-delay, the peak of the frequency-response plot shifts towards a higher frequency.

The location of the CPs on the frequency-response curves for different values of the time-delay can be analytically determined from

$$\frac{\partial}{\partial \tau}\left[\left|G(\mathrm{j}\omega)\right|\right] = 0. \tag{13}$$

Eq. (13) leads to the following expression for the *crossing frequency*:

$$\omega_{\mathrm{cross}} = \sqrt{\frac{1-R^2}{1-Rk_c-R^2}}. \tag{14}$$

It may be noted that the frequency response behaves oppositely below and above the *crossing frequency*. With the increasing value of the time-delay, the frequency response decreases and increases, respectively, below and above this frequency. Therefore, the near-resonance performance of the control system can be enhanced by shifting the *crossing frequency* towards the lower frequency range (far below unity) and using a small value of the time-delay. From Eq. (14), it is now known that ω_{cross} decreases with the increasing values R and $|k_c|$. Thus, the near-resonance response can be reduced by using higher values of R and k_c along with a small value of the time-delay. This qualitative conclusion is further substantiated by the following analytical expression of the controlled response at the resonance:

$$\left|G(\mathrm{j}\omega)\right|_{\omega=1} = \frac{\sqrt{1+R^2-2R\cos\tau}}{|k_c|}. \tag{15}$$

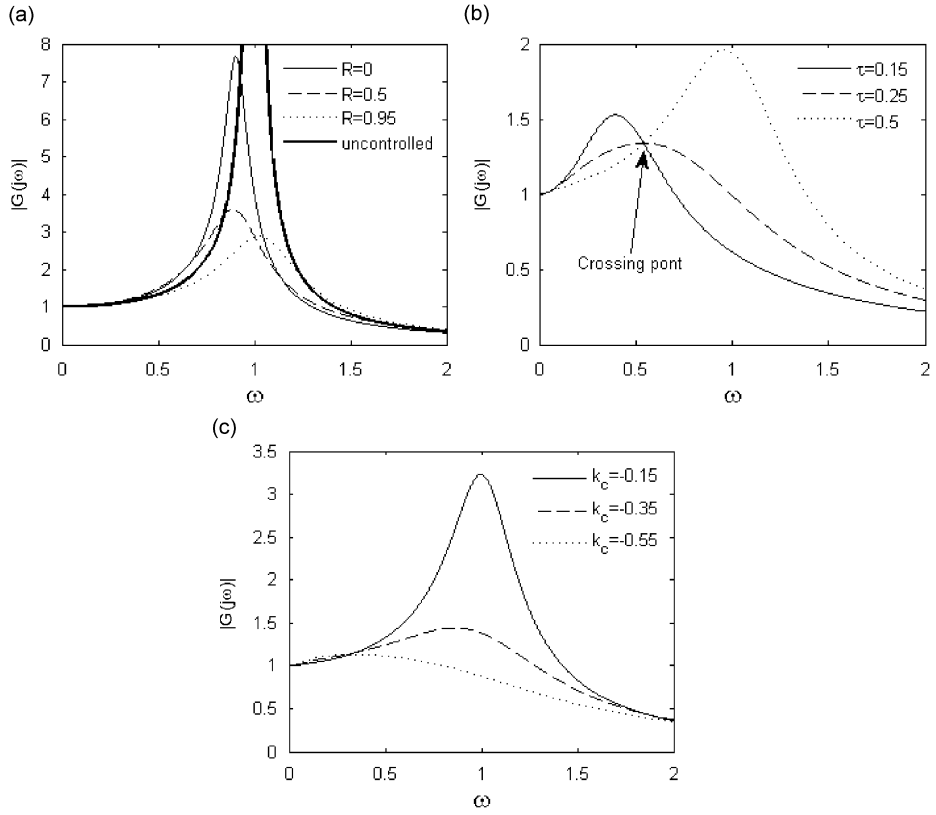

Fig. 3. Frequency-response plots for different parameter values: (a) $k_c = -0.25$, $\tau = 0.75$; (b) $k_c = -0.25$, $R = 0.95$; (c) $\tau = 0.5$, $R = 0.95$.

However, it is observed from the frequency-response characteristics shown in Fig. 3(b) that the reduced response near the resonance is achieved only at the cost of increased response in the low-frequency range (below ω_{cross}). Therefore, when the excitation spectrum contains low-frequency components, a tradeoff between the low-frequency response and the resonance response is required. Under these circumstances, the following discussion may be of great help in selecting the suitable values of the parameters.

It is apparent from the frequency-response plots (Fig. 3(b)) for different time-delays that the minimum possible peak of the frequency response over all time-delays is coincident with the CP at ω_{cross}. The corresponding value of the time-delay can be obtained by solving the following equation:

$$\frac{\partial}{\partial\omega}\left[\left|G(\mathrm{j}\omega,\tau)\right|\right]_{\omega=\omega_{\text{cross}},\tau=\tau_m} = 0 \tag{16}$$

with the condition

$$\frac{\partial^2}{\partial\omega^2}\left[\left|G(\mathrm{j}\omega,\tau)\right|\right]_{\omega=\omega_{\text{cross}},\tau=\tau_m} < 0. \tag{17}$$

Finally, the expression for the time-delay corresponding to the minimum response peak is derived as

$$\tau_m = \frac{1}{\omega_{\text{cross}}}\cos^{-1}\left[\frac{2R^3 + 3R^2k_c + Rk_c^2 - 2R - k_c}{R^4 + 2R^3k_c + R^2k_c^2 - 1}\right]. \tag{18}$$

Of course τ_m should be chosen from inside the primary stable region. However, the above formula is valid only for some smaller values of k_c beyond which the CP is not the global peak of the frequency-response plot for $\tau = \tau_m$. For higher values of k_c, the global peak appears elsewhere at a higher frequency (results are not shown).

Thus when the input spectrum has significant low-frequency contents, Eq. (18) provides a suitable value of the time-delay. Subsequently, the frequency-response characteristics may be favorably modified, if required, by fine-tuning the time-delay around the above initial estimate.

Case II*:* $R = 1$. From Eq. (14), it is noted that $\omega_{\text{cross}} = 0$ for $R = 1$. Thus, the frequency-response plots for different time-delays have only $\{0, |G(0)|\}$ as the common crossing point. This is advantageous because the vibration response can be controlled uniformly over the entire frequency band by decreasing the value of the time-delay. Typical frequency-response characteristics of the system for $R = 1$ are illustrated in Fig. 4. These frequency-response plots clearly reveal that the control systems with $R = 1$ and the smallest possible value of the time-delay as permissible by the hardware, are the most effective in controlling the resonant and non-resonant low- frequency vibrations.

Hitherto, only the displacement response of the system is considered. However, in vibration problems, other kinematic variables like velocity and acceleration are also of importance. Thus, it is worth exploring the frequency-response characteristics of these kinematic variables. It is established above that the controller with $R = 1$ and small delay offers the best frequency-response characteristics of the displacement. Fig. 5 shows the frequency-response plots of the displacement, velocity and acceleration of the system over a wide frequency band. It is observed from these plots that the displacement, velocity and acceleration response of the system improve to a great extent over a broad range of frequency around the resonance. However, the response increases marginally in the high-frequency range except at some specific narrow frequency bands, where the response becomes very low due to anti-resonances. These anti-resonances are typically associated with the specific form of the controller [21].

It is important to analyze the frequency-response plots of the control effort. The corresponding transfer function is defined as

$$G_c(s) = \frac{k_c U(s)}{F(s)} = \frac{k_c s^2}{(s^2+1)(1 - R\mathrm{e}^{-s\tau}) - k_c s^2 \mathrm{e}^{-s\tau}}, \tag{19}$$

where $U(s)$ and $F(s)$ are the Laplace transforms of $u(t)$ and $f(t)$, respectively.

Frequency-response plots of the control effort thus defined are shown in Fig. 6. It is easy to see from Eq. (19) that for any combination of the parameter values, the frequency-response plots of the control effort pass through a common point ($\omega = 1, |G_c(\mathrm{j}\omega)| = 1$), which is also apparent from Fig. 6. This implies that the

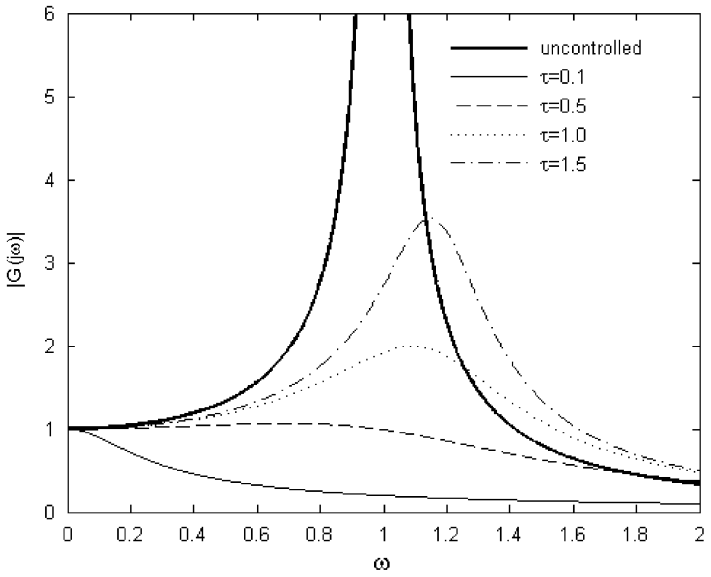

Fig. 4. Frequency-response plots of the controlled and uncontrolled system. $R = 1$, $k_c = -0.5$.

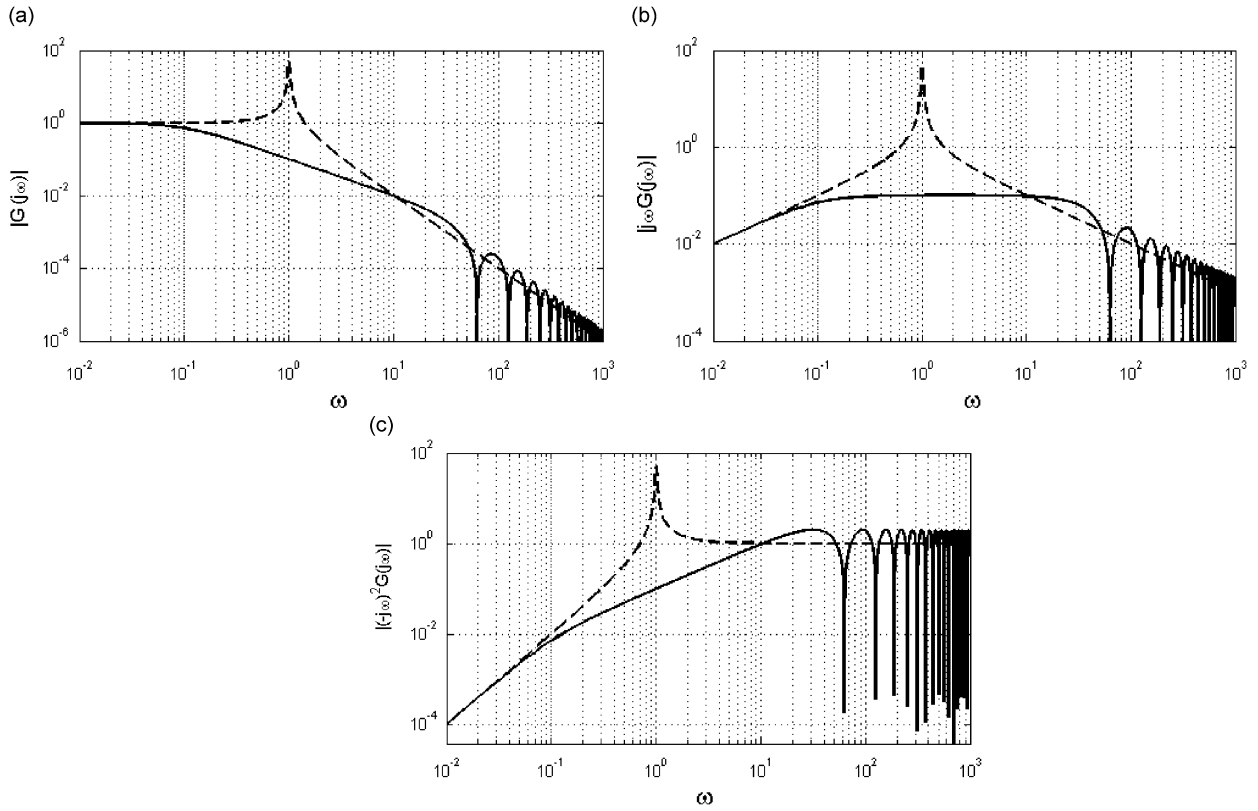

Fig. 5. Displacement, velocity and acceleration frequency-response plots. $R = 1$, $\tau = 0.1$, $k_c = -1.0$: (a) displacement; (b) velocity; (c) acceleration.----- uncontrolled; _____ controlled.

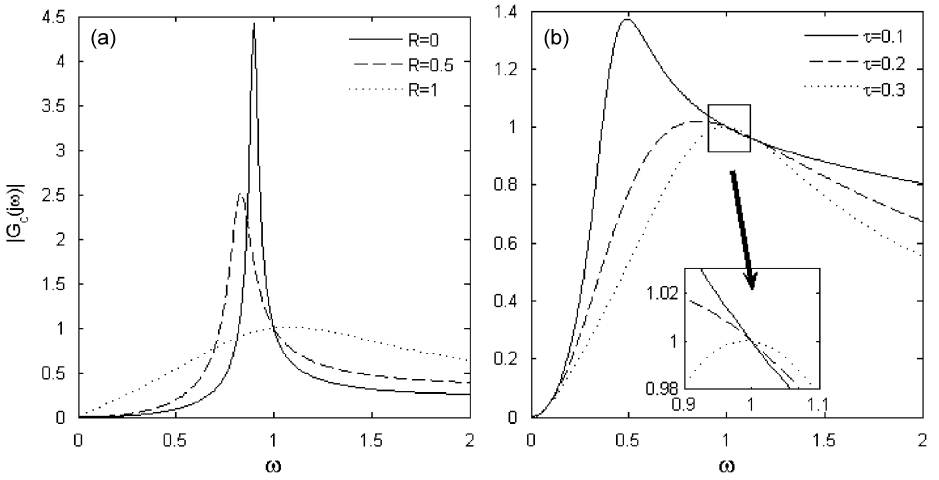

Fig. 6. Frequency-response plots of the control effort. $k_c = -0.25$: (a) $\tau = 0.25$; (b) $R = 0.95$.

control force required to mitigate the resonance response is of the same magnitude as the exciting force and cannot be changed by any parametric variation. However, the control parameters may be appropriately selected so as to minimize the maximum control effort for broad-band vibration control. Thus, the control actuator is susceptible to saturation and therefore, care must be exercised while selecting the control actuator.

The phase ϕ_c of the control effort with respect to the exciting force at $\omega = 1$ depends only on the delay parameter as evident from the following expression:

$$\phi_c = -\pi + \tau. \tag{20}$$

This explains why the near-resonance response decreases with the decreasing value of τ. Actually for lower values of τ, the control force acts almost in antiphase with the exciting force and tends to nullify its effect.

2.4. Equivalent damping and natural frequency

2.4.1. Harmonic estimate

In order to explain the above-discussed characteristics of the system in light of an equivalent second-order delay-free oscillator, the original time-delayed system is assumed to be driven by a simple harmonic input as $f(t) = F_0 \sin \omega t$. Then the equivalent delay-free system is described as a damped oscillator governed by the following equation:

$$m_e\ddot{y} + c_e\dot{y} + k_e y = F_0 \sin \omega t. \tag{21}$$

Obviously, the effective mass (m_e), damping (c_e) and the stiffness (k_e) parameter of the equivalent system should be frequency dependent. Substituting the assumed harmonic solution $x = A \sin(\omega t - \phi)$ into the original equation (Eq. (1)), the following expressions for the system parameters are obtained:

$$\begin{aligned} &m_e(\omega) = 1 - k_c C(\omega\tau), \\ &c_e(\omega) = -k_c \omega S(\omega\tau), \\ &\text{and} \\ &k_e = 1, \end{aligned} \tag{22}$$

where the functions $S(z)$ and $C(z)$ are defined as

$$S(z) = \sum_{k=1}^{\infty} R^{k-1} \sin(kz), \tag{23a}$$

$$C(z) = \sum_{k=1}^{\infty} R^{k-1} \cos(kz). \tag{23b}$$

Evidently, the delayed acceleration feedback modifies the inertial and damping properties of the system. Finally, Eq. (21) is recast into the following standard form:

$$\ddot{y} + 2\xi\omega_n\dot{y} + \omega_n^2 y = \tilde{F}_0 \sin \omega t, \tag{24}$$

where

the damping factor $\xi = -\dfrac{k_c \omega S(\omega\tau)}{2\sqrt{1 - k_c C(\omega\tau)}}$

the natural frequency $\omega_n = \dfrac{1}{\sqrt{1 - k_c C(\omega\tau)}}$,

and $\tilde{F}_0 = F_0 \omega_n^2$.

Variations of the effective damping factor and the natural frequency of the system with the time-delay are shown in Fig. 7. The functions $S(\omega\tau)$ and $C(\omega\tau)$ are computed according to Eq. (23a, b) with k running from 0 to 1000. For the values of R (<1) considered here, the series converges within this range of k. It is observed from Fig. 7 that increasing the value of R and selecting a suitable value of the time-delay, can enhance the maximum value of the effective damping factor. The value of the time-delay corresponding to the maximum damping decreases with the increasing value of R. The effective natural frequency of the system increases with the time-delay. It is important to note that for higher values of R and smaller values of the time-delay, the effective natural frequency shifts significantly towards the low-frequency region. The combined effects of

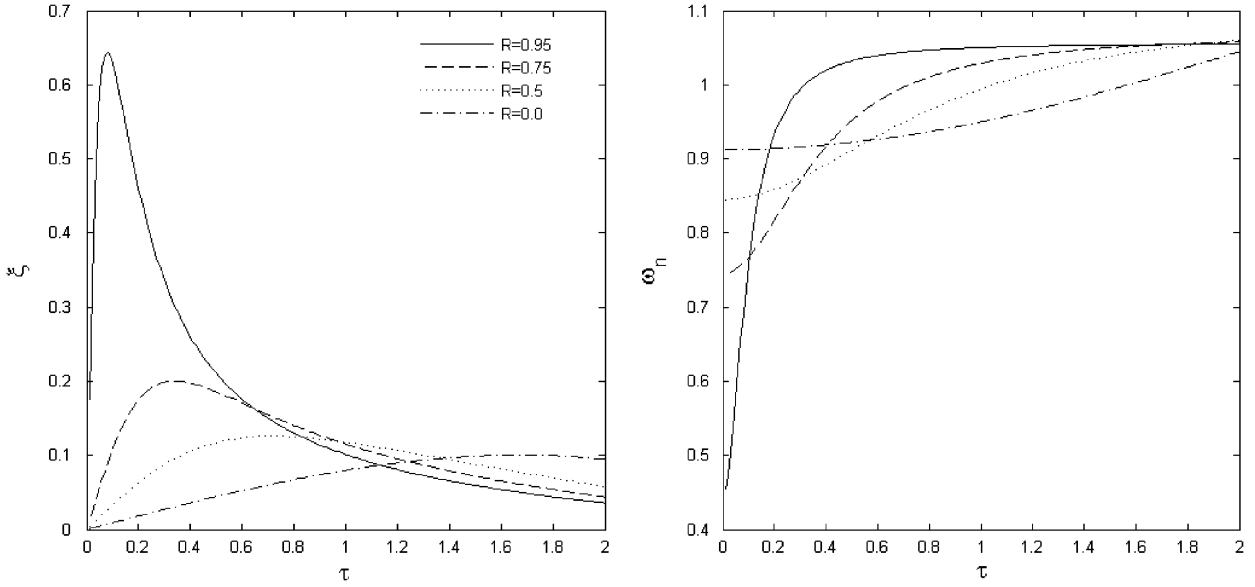

Fig. 7. Variations of the equivalent damping factor and natural frequency with delay. $\omega = 1$, $k_c = -0.2$.

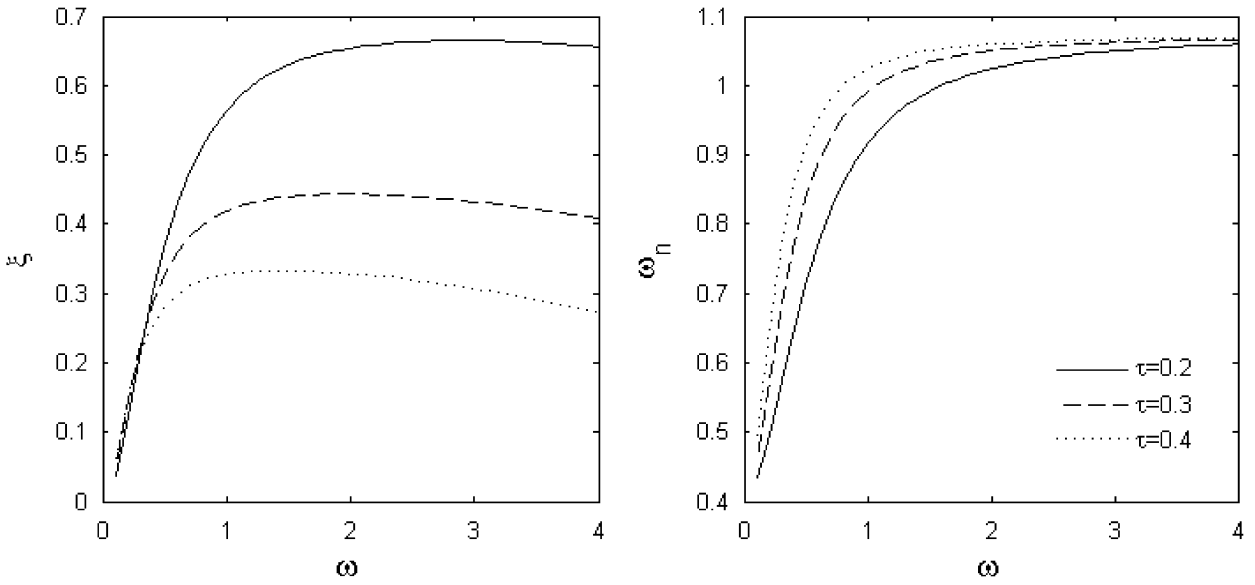

Fig. 8. Frequency dependence of the damping factor and the natural frequency. $k_c = -0.25$, $R = 0.95$.

the increasing effective damping and the decreasing natural frequency with the increasing value of R and the corresponding optimum values of the time-delay are instrumental in controlling the resonant vibration.

The harmonic estimates of the effective damping factor and the natural frequency are evidently functions of the operating frequency. Fig. 8 shows the variations of the damping factor and natural frequency with the operating frequency.

One must note that $S(z)$ and $C(z)$ defined in Eqs. (23a,b) are not convergent functions for $R = 1$ and hence the concept of equivalent damping is not applicable in this case. In the following, an alternative approximate description of the system applicable to all values of R is presented.

2.4.2. Equivalent lower order system

The exponential term in Eq. (4) can be replaced by the following Pade approximant for small values of the time-delay:

$$e^{-s\tau} = \frac{2 - s\tau}{2 + s\tau}. \tag{25}$$

Substituting Eq. (25) into Eq. (4), yields the following simplified expression of the transfer function:

$$G(s) = \frac{2(1 - R) + (1 + R)s\tau}{(1 + R + k_c)\tau s^3 + 2(1 - R - k_c)s^2 + (1 + R)\tau s + 2(1 - R)}. \tag{26}$$

The transfer function given in Eq. (26) is an approximate third-order representation of the original infinite order system given by Eq. (4). The approximate system has either one real pole and a pair of complex conjugate poles or three real poles.

For the first case, the approximate transfer function (26) can be recast as

$$G(s) = \frac{k_0(s - z_0)}{(s + p_0)(s^2 + 2\xi\omega_n s + \omega_n^2)}, \tag{27}$$

where k_0 is a real constant.

The real zero of the stable system is $z_0 = -2(1 - R)/\tau(1 + R)$, which lies on the negative real axis for $R < 1$. The real zero approaches the origin with the increasing value of the time-delay and R. The real pole p_0 is clearly a non-system pole and the quadratic factor provides the system poles with the damping factor ξ and the natural frequency ω_n. Variations of the damping factor and the natural frequency of the system with the time-delay are depicted in Figs. 9 and 10. It is observed from Fig. 9 that for fixed values of R (<1) and k_c, the damping factor first increases with the time-delay and then decreases after an optimum value of the time-delay when the damping factor assumes the maximum value. The maximum damping factor and the corresponding optimum value of the time-delay increase with the control gain. It is observed from Fig. 10 that while the maximum damping factor increases, the optimum value of the time-delay decreases with the increasing value of R. From Fig. 10, it is apparent that the natural frequency of the system increases with the time-delay. In the small delay region, the effective natural frequency of the system decreases with the increasing values of the control gain and R. It is not difficult to show (see Appendix A) that for $R < 1$, $\xi \propto \tau$ in the small delay limit. These observations are qualitatively consistent with that made in Section 2.4.1.

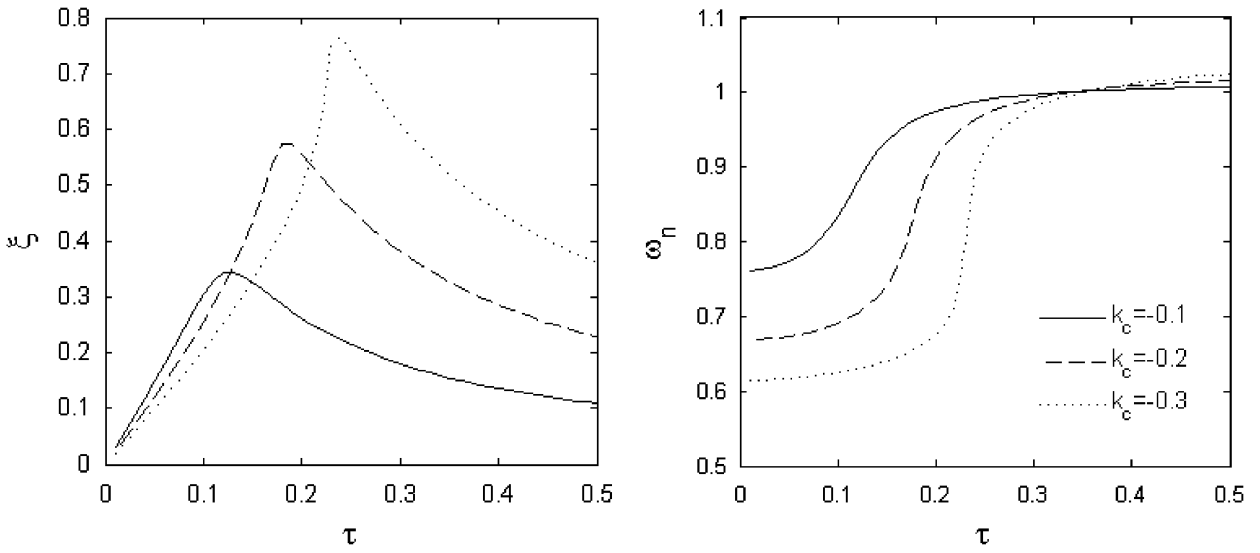

Fig. 9. Variations of the damping factor and the natural frequency with delay for various control gain. $R = 0.95$.

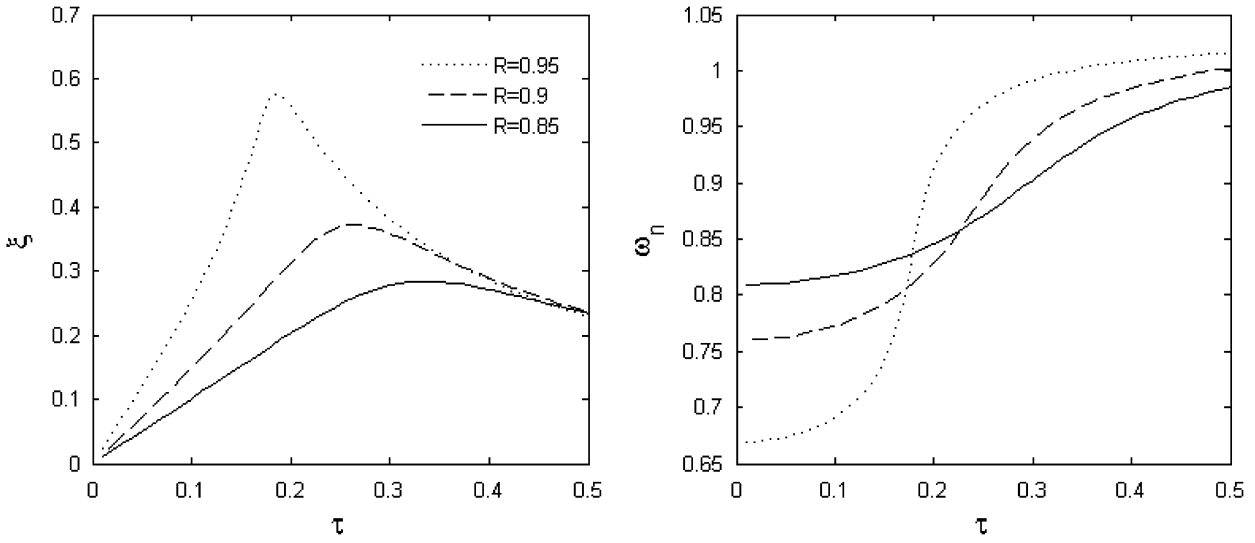

Fig. 10. Variations of damping factor and natural frequency with delay for various R. $k_c = -0.2$.

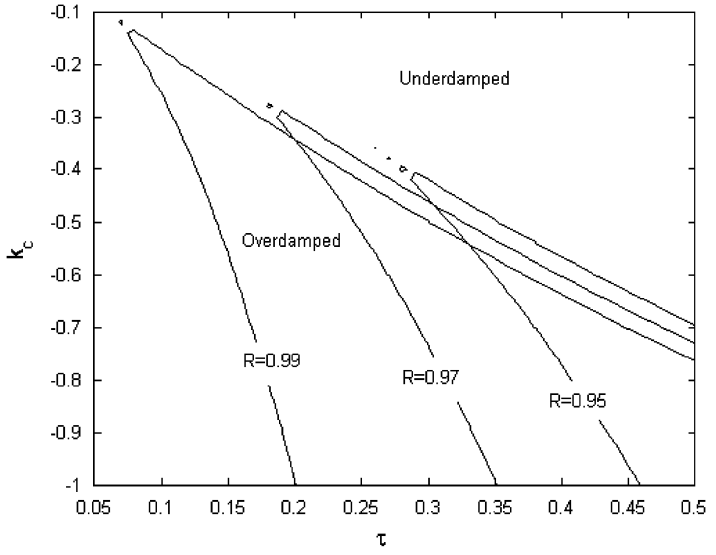

Fig. 11. Regions of overdamped and underdamped conditions.

When all poles of the transfer function (26) are real, the system becomes overdamped, i.e. $\xi > 1$. The regions of the overdamped and underdamped conditions in the parameter plane are depicted in Fig. 11. It is observed from Fig. 11 that the system tends to become overdamped for large values of R and k_c.

For $R = 1$, Eq. (26) is rewritten as

$$G(s) = \frac{2s\tau}{s\{(2 + k_c)\tau s^2 - 2k_c s + 2\tau\}}. \tag{28}$$

It is evident from Eq. (28) that when $R = 1$, a pole and a zero at the origin cancels each other and the system effectively behaves like a second-order system. Comparing Eq. (28) with the standard form of a second-order system

$$G(s) = \frac{\omega_n^2}{s^2 + 2\xi\omega_n s + \omega_n^2}, \tag{29}$$

the following expressions for the damping factor ξ and the natural frequency ω_n are obtained:

$$\xi = \frac{|k_c|}{2\tau}\sqrt{\frac{2}{2-|k_c|}}, \tag{30}$$

$$\omega_n = \sqrt{\frac{2}{2-|k_c|}}. \tag{31}$$

From the above analysis, it is understood that the system undergoes an important characteristic change at $R=1$. Eq. (30) reveals that the effective damping factor is inversely proportional to the time-delay, particularly in the small delay limit (note that the Pade approximant is more accurate in the small delay region). Interestingly, this is in contrast with that observed for $R<1$ where the damping factor is proportional to the time-delay in the small delay limit. From Eqs. (30) and (31), it is evident that both the effective damping factor and the natural frequency of the system increase with the control gain, but the natural frequency remains independent of the time-delay. Thus, the effective damping of the system can be increased without changing the natural frequency by decreasing the time-delay. Although these results are theoretically very interesting, there are obvious practical limitations in using a very low value of the delay, particularly in fast systems.

2.5. Transient response and pole-zero configuration

The concept of the equivalent damping can help select the optimum values of the control parameters for controlling forced vibrations. However, the locations of the poles and zeros of the closed-loop system determine the exact shape of the transient response. In Section 2.4.1, an approximate lower order system sheds some light on the pole-zero configuration of the system. It is known that for $R<1$, a real non-system zero and pole move towards the imaginary axis with the increasing value of the delay. However, these results are valid only for some small values of the delay parameter. In the following, a relatively complete analysis, valid for any value of the time-delay, is presented.

Substituting $s=\sigma+\mathrm{j}\omega$ into the characteristics equation (Eq. (5)) and separating the real and imaginary parts, yield

$$1+\sigma^2-\omega^2-p_1(\sigma,\omega)\mathrm{e}^{-\sigma\tau}\cos\omega\tau-p_2(\sigma,\omega)\mathrm{e}^{-\sigma\tau}\sin\omega\tau=0, \tag{32}$$

$$2\sigma\omega+p_1(\sigma,\omega)\mathrm{e}^{-\sigma\tau}\sin\omega\tau-p_2(\sigma,\omega)\mathrm{e}^{-\sigma\tau}\cos\omega\tau=0, \tag{33}$$

where σ is the real part and ω is the imaginary part of a pole,

$$p_1(\sigma,\omega)=R+(\sigma^2-\omega^2)(R+k_c)$$

and

$$p_2(\sigma,\omega)=2\sigma\omega(R+k_c).$$

The poles of the system are obtained by solving Eqs. (32) and (33) for σ and ω, whereas zeros are obtained from Eq. (11). However, only the poles and zeros near the imaginary axis are of importance. It is apparent from Eq. (33) that $\omega=0$ is a possible solution, which implies the existence of purely real poles. Substituting $\omega=0$ into Eq. (32), yields

$$1+\sigma^2-\mathrm{e}^{-\sigma\tau}\left[R+\sigma^2(R+k_c)\right]=0. \tag{34}$$

The real poles are obtained by solving Eq. (34), which has real solutions for the values of R close to unity. The zero on the real line is obtained from Eq. (11) as

$$z_0=\frac{\ln(R)}{\tau}. \tag{35}$$

It is well known that the distance between a pole and its nearest zero determines the degree of dominance of the particular pole in the transient response of the system. The effect of a pole on the system dynamics can be

nullified by a nearby zero. In order to measure the distance of the real zero from the real poles of the system, the absolute value of the left-hand side expression of Eq. (34) is evaluated at $\sigma = z_0$ as

$$E(\tau) = \frac{|k_c|\{\ln(R)\}^2}{R\tau^2}. \tag{36}$$

Obviously, very low values of E imply the existence of a real pole close to z_0. Evidently, E tends to zero when R approaches unity and the delay increases. Thus with the increasing value of R andτ, the real pole and the zero shift closer to the imaginary axis and also to each other. Note that E is exactly zero at $R = 1$ when the real pole and the zero meet at the origin.

A real pole close to the imaginary axis controls the maximum overshoot in the transient response. However, if the real pole is the dominant one, transient response becomes sluggish. With the increasing delay, a real pole of the system tends towards the imaginary axis and hence becomes the dominant one. But the effect of this pole is nullified by the real zero, which is also approaching the imaginary axis with the increasing delay. Though exact pole-zero cancellation is never possible for $R<1$, one can optimally select the gain k_c and the time-delay τ such that the effect of the dominant real pole is nullified to a great extent by a nearby zero. This is particularly possible when R is chosen close to unity. Under these circumstances, the damping of the system is governed by the pole having the second largest absolute value of the real part. Such an optimum selection is indeed possible as illustrated in Fig. 12. From this figure, it is clearly observed that $k_c = -1$ and $\tau = 1$ is the optimum choice for $R = 0.95$. For these choices of the parameters, the effect of the dominant pole is clearly suppressed by the nearby zero.

For $R = 1$, the real zero and the pole at the origin exactly cancels each other. Thus, the damping of the system is governed by the dominant pole(s) with non-trivial negative real part(s). The map of the dominant

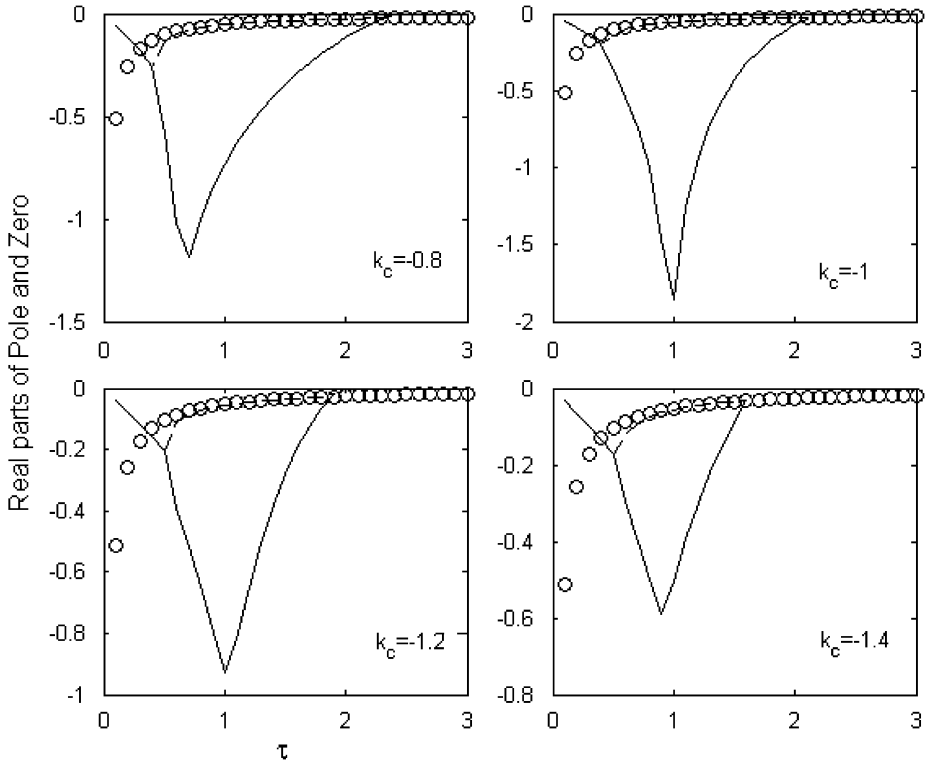

Fig. 12. Variations of the real parts of the pole and zero with delay. ○, real zero;- - -, largest real part of poles (real); ___, second largest real part of poles (complex). $R = 0.95$.

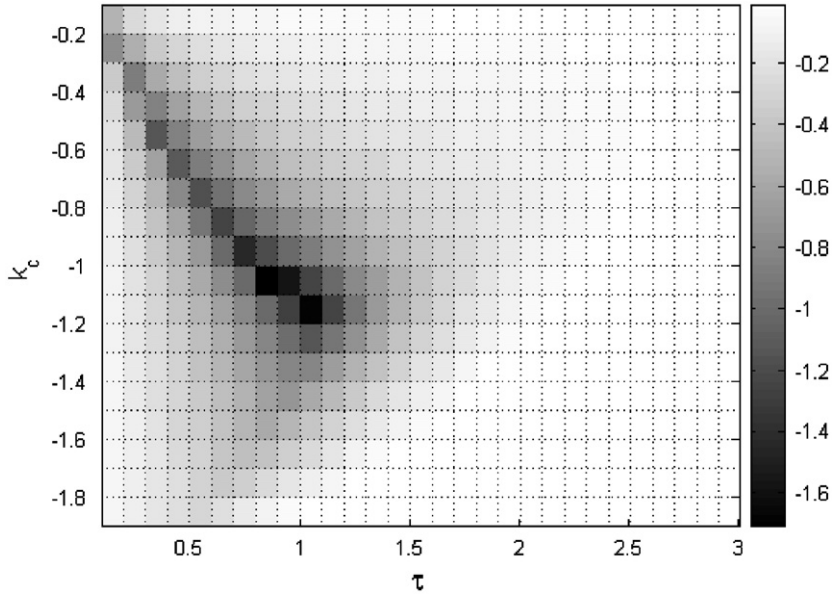

Fig. 13. Map of the negative real part of the dominant pole. $R = 1$.

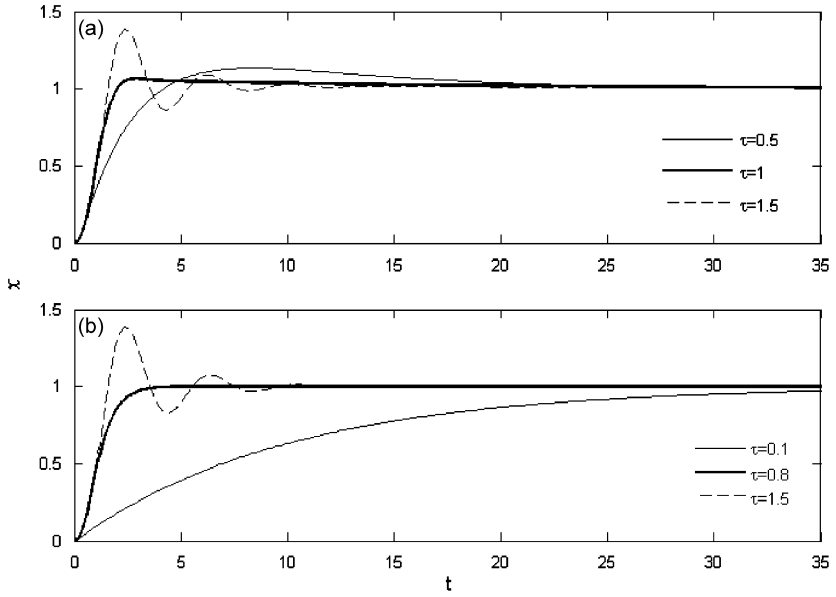

Fig. 14. Time history plots of the transient response obtained by direct numerical simulation. $k_c = -1$: (a) $R = 0.95$, (b) $R = 1$.

stable real part is shown in Fig. 13, which confirms the existence of an optimal choice of k_c and τ corresponding to the darkest regions.

Numerically simulated transient responses of the system under unit step input are shown in Fig. 14. These plots apparently substantiate the discussions and observations made above.

It is worth noting that the optimum choices of the time-delay parameter for controlling forced vibrations may be different (depends on the gain) from that required for controlling transient vibrations. When both are important, a suboptimal choice of the delay parameter can be made. However, in both the cases, $R = 1$ is the best choice.

3. Controlling nonlinear vibration

In this section, the efficacy of the extended time-delayed acceleration feedback control of a Duffing oscillator is considered. The non-dimensional equation of motion of the system is given as

$$\begin{aligned} &\ddot{x} + x + k_3 x^3 = f_0 \cos \omega t + k_c u, \\ &u = \ddot{x}(t-\tau) + Ru(t-\tau) = \sum_{k=1}^{\infty} R^{k-1} \ddot{x}(t-k\tau), \end{aligned} \tag{37}$$

where k_3 is the coefficient of the cubic term, f_0 the strength and ω the frequency of excitation.

Also it is assumed that the nonlinearity, excitation and control forces are weak. Then it is pertinent to write $k_3 = \varepsilon \tilde{k}_3$, $f_0 = \varepsilon \tilde{f}$ and $k_c = \varepsilon \tilde{k}_c$, where ε ($\ll 1$) is a small quantity.

3.1. Controlling primary resonance

Here, the dynamics of the controlled oscillator near the primary resonance is considered. Towards this end, the method of multiple time scales is used. For simplicity, a two-scale expansion of the solution is expressed as

$$x = x_0(T_0, T_1) + \varepsilon x_1(T_0, T_1), \tag{38}$$

where the two time scales for expansion are taken as $T_0 = t$, $T_1 = \varepsilon t$.

Note that

$$\begin{aligned} \frac{\mathrm{d}x}{\mathrm{d}t} &= \frac{\partial x}{\partial T_0} + \varepsilon \frac{\partial x}{\partial T_1}, \\ \frac{\mathrm{d}^2 x}{\mathrm{d}t^2} &= \frac{\partial^2 x}{\partial T_0^2} + 2\varepsilon \frac{\partial^2 x}{\partial T_0 \partial T_1} + \varepsilon^2 \frac{\partial^2 x}{\partial T_1^2}. \end{aligned} \tag{39}$$

As the solution near the primary resonance is of major concern, the excitation frequency is perturbed around unity, i.e.

$$\omega = 1 + \varepsilon \delta, \tag{40}$$

where δ is the detuning parameter.

Perturbing the solution around the primary resonance yields

$$\frac{\partial^2 x_0}{\partial T_0^2} + x_0 = 0, \tag{41}$$

$$\frac{\partial^2 x_1}{\partial T_0^2} + x_1 = -2\frac{\partial^2 x_0}{\partial T_0 \partial T_1} - \tilde{k}_3 x_0^3 + \tilde{k}_c \sum_{k=1}^{\infty} \left[R^{k-1} \frac{\partial^2}{\partial T_0^2} \{ x_0(T_0 - k\tau) \} \right] + \tilde{f} \cos(T_0 + \delta T_1). \tag{42}$$

The general solution of Eq. (41) is written as

$$x_0(T_0, T_1) = A(T_1) \mathrm{e}^{\mathrm{i}T_0} + \text{c.c.}, \tag{43}$$

where c.c. denotes the complex conjugate part of the solution and

$$A(T_1) = \tfrac{1}{2} \alpha(T_1) \mathrm{e}^{\mathrm{i}\beta(T_1)} \tag{44}$$

with $\alpha(T_1)$ and $\beta(T_1)$ are two real functions.

Substituting Eq. (43) into Eq. (42), yields

$$\frac{\partial^2 x_1}{\partial T_0^2} + x_1 = -2\frac{\partial}{\partial T_1} \left[\mathrm{i} A \mathrm{e}^{\mathrm{i}T_0} \right] - \tilde{k}_3 \left[A^3 \mathrm{e}^{3\mathrm{i}T_0} + 3A^2 \bar{A} \mathrm{e}^{\mathrm{i}T_0} \right] - \tilde{k}_c \sum_{k=1}^{\infty} R^{k-1} A \mathrm{e}^{\mathrm{i}T_0} \mathrm{e}^{-\mathrm{i}k\tau} + \frac{\tilde{f}}{2} \mathrm{e}^{\mathrm{i}\delta T_1} \mathrm{e}^{\mathrm{i}T_0} + \text{c.c.} \tag{45}$$

The secular terms in the right-hand side of Eq. (45) vanish if

$$-2\mathrm{i}\frac{\partial A}{\partial T_1} - 3\tilde{k}_3 A^2 \bar{A} - \tilde{k}_c \sum_{k=1}^{\infty} R^{k-1} A \mathrm{e}^{-\mathrm{i}k\tau} + \frac{\tilde{f}}{2}\mathrm{e}^{\mathrm{i}\delta T_1} = 0. \tag{46}$$

Substituting Eq. (44) into Eq. (46) and separating the real and imaginary parts, yield

$$\alpha \frac{\mathrm{d}\varphi}{\mathrm{d}T_1} = \alpha\delta - \frac{3}{8}\tilde{k}_3\alpha^3 - \frac{\tilde{k}_c}{2}\alpha C(\tau) + \frac{\tilde{f}}{2}\cos\,\varphi, \tag{47}$$

$$\frac{\mathrm{d}\alpha}{\mathrm{d}T_1} = \frac{\tilde{k}_c}{2}\alpha S(\tau) + \frac{\tilde{f}}{2}\sin\,\varphi, \tag{48}$$

where $\varphi = \delta T_1 - \beta$ and the functions $C(\tau)$ and $S(\tau)$ are as defined in Eq. (23a,b). It may be remembered that these functions are only valid for $R<1$.

The steady-state solutions (α_0, φ_0) of Eqs. (47) and (48) are obtained by solving the following two nonlinear algebraic equations:

$$\alpha_0\delta - \frac{3}{8}\tilde{k}_3\alpha_0^3 - \frac{\tilde{k}_c}{2}\alpha_0 C(\tau) + \frac{\tilde{f}}{2}\cos\,\varphi_0 = 0, \tag{49}$$

$$\frac{\tilde{k}_c}{2}\alpha_0 S(\tau) + \frac{\tilde{f}}{2}\sin\,\varphi_0 = 0. \tag{50}$$

Squaring and adding Eqs. (49) and (50), yield

$$\alpha_0^2\left[\left\{\delta - \frac{3}{8}\tilde{k}_3\alpha_0^2 - \frac{\tilde{k}_c}{2}C(\tau)\right\}^2 + \left\{\frac{\tilde{k}_c}{2}S(\tau)\right\}^2\right] = \frac{\tilde{f}^2}{4}. \tag{51}$$

Eq. (49) may be recast as a cubic equation of $y = \alpha_0^2$

$$a_3 y^3 + a_2 y^2 + a_1 y + a_0 = 0, \tag{52}$$

where

$$a_3 = \frac{9}{64}\tilde{k}_3^2,\ a_2 = -\frac{3}{4}\left(\delta - \frac{\tilde{k}_c}{2}C\right)\tilde{k}_3,\ a_1 = \left(\delta - \frac{\tilde{k}_c}{2}C\right)^2 + \left(\frac{\tilde{k}_c}{2}S\right)^2 \text{ and } a_0 = -\frac{\tilde{f}^2}{4}.$$

Now the first-order approximate solution of the response near the primary resonance of the system is written as

$$x(t) = \alpha_0\,\cos(\omega t - \phi_0) + O(\varepsilon), \tag{53}$$

where α_0 is obtained by solving Eq. (52), which has either three real solutions or one real solution. The phase ϕ_0 is obtained from the following equation:

$$\tan\,\phi_0 = \frac{\tilde{k}_c\alpha_0 S(\tau)}{2\alpha_0\delta - \frac{3}{4}\tilde{k}_3\alpha_0^3 - \tilde{k}_c\alpha_0 C(\tau)}. \tag{54}$$

Stabilities of the above steady-state solutions are ascertained by the eigenvalues of the Jacobian of the linearized slow flow equations (Eqs. (47) and (48)) in the neighborhood of the steady-state solutions given below:

$$\begin{Bmatrix} \frac{\mathrm{d}\alpha}{\mathrm{d}T_1} \\ \frac{\mathrm{d}\varphi}{\mathrm{d}T_1} \end{Bmatrix} = \begin{bmatrix} \frac{1}{2}\tilde{k}_c S_2(\tau) & \frac{1}{2}\tilde{f}\,\cos\,\varphi_0 \\ -\frac{3}{4}\tilde{k}_3\alpha_0 - \frac{\tilde{f}\,\cos\,\varphi_0}{2\alpha_0^2} & \frac{\tilde{f}\,\sin\,\varphi_0}{2\alpha_0^2} \end{bmatrix} \begin{Bmatrix} \alpha \\ \varphi \end{Bmatrix}. \tag{55}$$

The characteristic equation associated with the coefficient matrix of Eq. (55) is quadratic in nature and is written as

$$b_2\eta^2 + b_1\eta + b_0 = 0, \tag{56}$$

where

$$b_2 = 1,$$
$$b_1 = -\tilde{k}_c S(\tau),$$
$$b_0 = \left(\frac{b_1}{2}\right)^2 + \left(-\delta + \frac{\tilde{k}_c}{2}C(\tau) + \frac{3}{8}\tilde{k}_3\alpha_0^2\right)\left(-\delta + \frac{\tilde{k}_c}{2}C(\tau) + \frac{9}{8}\tilde{k}_3\alpha_0^2\right).$$

A solution is stable if and only if $b_1, b_2 > 0$. Note that the first stability condition $b_1 > 0$ is also the condition of the stability of the trivial equilibrium.

Typical frequency-response plots of the primary resonance of the system are shown in Fig. 15. It is learnt from these frequency-response plots that more damping can be produced by increasing the value of R and appropriately selecting the time-delay. In case of linear systems, it is shown that the near-resonance performance can be improved by selecting higher values of R and correspondingly smaller values of the time-delay. This conclusion holds good also for nonlinear systems.

From Eq. (51), the maximum value of the primary resonance amplitude α_0 is readily obtained as

$$(\alpha_0)_{\max} = -\frac{\tilde{f}}{\tilde{k}_c S(\tau)} = \frac{\tilde{f}}{b_1}. \tag{57}$$

Eq. (57) clearly reveals that the increasing value of the product $b_1 = \tilde{k}_c S(\tau)$ controls the amplitude of the primary resonance response.

It is well known that the response of the Duffing oscillator may be multivalued and this is revealed as the hysteresis or jump in the frequency-response plot. The occurrence of jump depends on the strength of the excitation. In the present problem, the critical force required for jump to occur is obtained as

$$f_c = \sqrt{-\frac{8(\tilde{k}_c S(\tau))^3}{3\tilde{k}_3}} = \sqrt{\frac{8b_1^3}{3\tilde{k}_3}}. \tag{58}$$

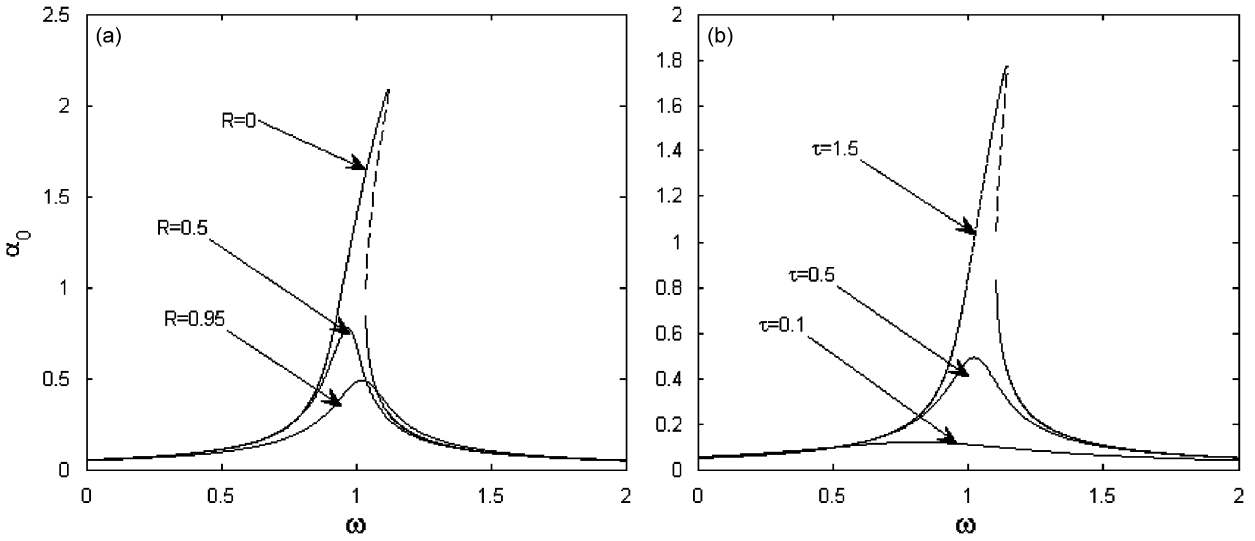

Fig. 15. Frequency-response plots of the Duffing oscillator near the primary resonance. Solid lines represent stable response and dashed lines represent unstable response. $k_3 = 0.1$, $k_c = -0.1$, $f_0 = 0.1$: (a) $\tau = 0.5$; (b) $R = 0.95$.

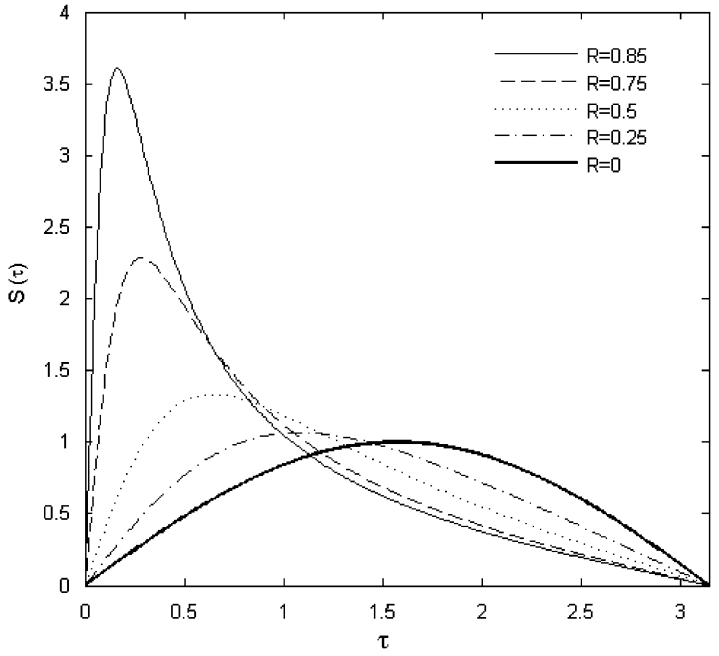

Fig. 16. Variations of the S-function with delay for different values of R.

Thus, the critical force required for jump increases with b_1. From Eqs. (57) and (58), it is now evident that b_1 plays the key role in controlling the primary resonance response of the Duffing oscillator. Thus, the resonance response can be improved by increasing control gain k_c and selecting τ such that the value of the function $S(\tau)$ is the maximum. Variations of the function $S(\tau)$ with τ are shown in Fig. 16 for various choices of R. Similar to what has been observed in case of linear systems, here also the optimal value of the time-delay decreases with the increasing value of R and the optimum value of the equivalent damping increases with R.

As mentioned earlier, the perturbation analysis described above is valid for $R<1$. It shown that when $R=1$, the equivalent damping of a linear system is inversely proportional to the time-delay in the small delay limit. For nonlinear systems, a similar result can be easily comprehended.

3.2. Controlling 1/3 subharmonic resonance

It is well known that the 1/3 subharmonic resonance is typical in a strongly excited Duffing oscillator. The efficacy of the proposed method in controlling this resonance is discussed in this section. Discussions are confined to weak nonlinearity, weak control and strong excitation. Thus, $k_3=\varepsilon\tilde{k}_3$ and $k_c=\varepsilon\tilde{k}_c$, where ε ($\ll 1$) is a small quantity. For analyzing the 1/3 subharmonic resonance, the operating frequency should be perturbed around 3. Therefore,

$$\omega = 3+\varepsilon\delta. \tag{59}$$

Proceeding as before, a two-scale expansion of the solution similar to Eq. (38) may be written where

$$\frac{\partial^2 x_0}{\partial T_0^2}+x_0=f_0\cos(3T_0+\delta T_1) \tag{60}$$

and

$$\frac{\partial^2 x_1}{\partial T_0^2}+x_1=-2\frac{\partial^2 x_0}{\partial T_1\partial T_0}-\tilde{k}_3x_0^3+\tilde{k}_c\sum_{k=1}^{\infty}R^{k-1}\ddot{x}_0(T_0-k\tau,T_1). \tag{61}$$

The solution of Eq. (60) is written as

$$x_0 = A(T_1)e^{iT_0} + Me^{i(3T_0+\delta T_1)} + \text{c.c.}, \tag{62}$$

where

$$M = \frac{f_0}{2(1-\omega^2)}.$$

Substituting Eq. (62) into (61) yields

$$\frac{\partial^2 x_1}{\partial T_0^2} + x_1 = -\left(2i\frac{dA}{dT_1} + 6\tilde{k}_3 AM^2 + 3\tilde{k}_3 A^2\bar{A}\right)e^{iT_0} - \tilde{k}_c A e^{iT_0}\sum_{k=1}^{\infty} R^{k-1}e^{-ik\tau} - 3\tilde{k}_3\bar{A}^2 M e^{i\delta T_1}e^{iT_0} + \cdots, \tag{63}$$

where $\bar{A}$ is the complex conjugate of A.

Removing the secular terms from the right-hand side of Eq. (63), yields

$$\left(2i\frac{dA}{dT_1} + 6\tilde{k}_3 AM^2 + 3\tilde{k}_3 A^2\bar{A}\right) + \tilde{k}_c A\sum_{k=1}^{\infty} R^{k-1}e^{-ik\tau} + 3\tilde{k}_3\bar{A}^2 M e^{i\delta T_1} = 0. \tag{64}$$

Writing A in the same form as in Eq. (44), the following two equations are obtained from Eq. (64):

$$\frac{d\alpha}{dT_1} = -\frac{3}{4}\tilde{k}_3 M\alpha^2 \sin\phi + \frac{1}{2}\tilde{k}_c\alpha S(\tau) \tag{65}$$

and

$$\frac{d\phi}{dT_1} = \delta - \frac{1}{2}\tilde{k}_c C(\tau) - 9\tilde{k}_3 M^2 - \frac{9}{8}\tilde{k}_3\alpha^2 - \frac{9}{4}\tilde{k}_3 M\alpha\cos\phi, \tag{66}$$

where $\phi = \delta T_1 - 3\beta$.

The steady-state solutions of Eqs. (65) and (66) are obtained by solving the following sets of nonlinear equations for α_0, ϕ_0:

$$-\tfrac{3}{4}\tilde{k}_3 M\alpha_0^2 \sin\phi_0 + \tfrac{1}{2}\tilde{k}_c\alpha_0 S(\tau) = 0, \tag{67}$$

$$\delta - \frac{1}{2}\tilde{k}_c C(\tau) - 9\tilde{k}_3 M^2 - \frac{9}{8}\tilde{k}_3\alpha_0^2 - \frac{9}{4}\tilde{k}_3 M\alpha_0\cos\phi_0 = 0. \tag{68}$$

Eliminating ϕ_0 from Eqs. (67) and (68), the following biquadratic equation in α_0 is obtained:

$$\alpha_0^4 - 2c_2\alpha_0^2 + c_0 = 0, \tag{69}$$

where

$$c_2 = \frac{8}{9\tilde{k}_3}\left[\delta - \frac{\tilde{k}_c C(\tau)}{2}\right] - 6M^2$$

and

$$c_0 = \frac{64}{81\tilde{k}_3^2}\left[\left\{\delta - \frac{1}{2}\tilde{k}_c C(\tau) - 9\tilde{k}_3 M^2\right\}^2 + \frac{9}{4}\tilde{k}_c^2 S^2(\tau)\right].$$

Now the first-order approximation of the 1/3 subharmonic response is written as

$$x(t) = \alpha_0\cos\left(\frac{\omega t - \phi_0}{3}\right) + \frac{f_0}{1-\omega^2}\cos\omega t. \tag{70}$$

The amplitude of 1/3 subharmonic component α_0 is obtained by solving Eq. (69) as

$$\alpha_0 = \sqrt{c_2 \pm \sqrt{c_2^2 - c_0}}. \tag{71}$$

The phase ϕ_0 is obtained from the following equation:

$$\tan\ \phi_0 = \frac{3\tilde{k}_c S(\tau)}{2\delta - \tilde{k}_c C(\tau) - 18\tilde{k}_3\alpha_0^2 - 9/4\tilde{k}_3 M\alpha_0}. \tag{72}$$

The stability of the two solutions thus obtained is ascertained by the eigenvalues of the linearized flow of the slow-flow equations (Eqs. (65), (66)) in the neighborhood of the respective steady-state solutions.

The conditions of the existence of the 1/3 subharmonic resonance are derived from Eq. (71) as $c_2 > 0$ and $c_2^2 > c_0$. After some algebraic manipulations, these conditions are finally recast as

$$\frac{32(\omega-3)M^2}{9k_3} - \frac{16k_c C(\tau)M^2}{9k_3} - \frac{16k_c^2 S^2(\tau)}{k_3^2} - 28M^4 \geqslant 0. \tag{73}$$

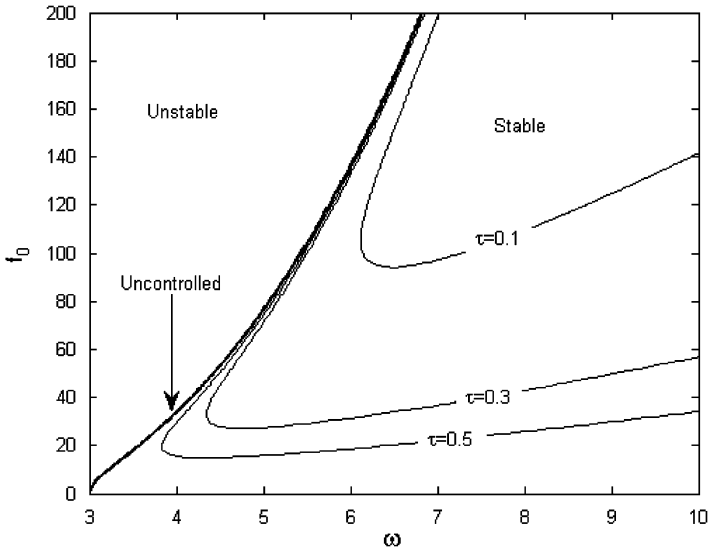

Fig. 17. Regions of existence of 1/3 subharmonic response. $k_3 = 0.1$, $R = 0.95$, $k_c = -0.1$.

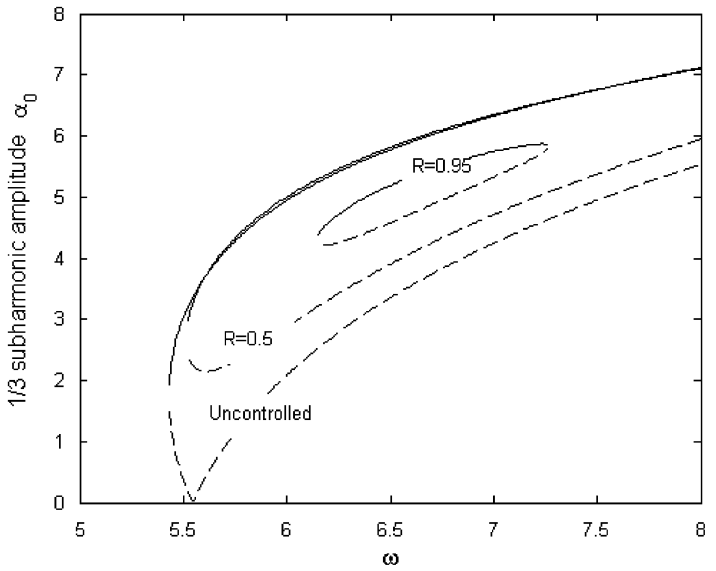

Fig. 18. Frequency response of 1/3 subharmonic amplitude. $f_0 = 100$, $k_3 = 0.1$, $k_c = -0.1$, $\tau = 0.1$. Solid lines and dashed lines represent the stable and unstable solutions, respectively.

The regions of existence of the 1/3 subharmonic response are depicted in Fig. 17 for different values of the time-delay. It is apparent from Fig. 17 that the amplitude of excitation required for the appearance of the 1/3 subharmonic resonance can be increased by appropriately choosing the control parameters. Again it is confirmed that the 1/3 subharmonic resonance can be suppressed by higher values of R and correspondingly lower values of the time-delay. Frequency-response plots of the 1/3 subharmonic amplitude are also shown in Fig. 18. Evidently, the amplitude of the 1/3 subharmonic resonance can also be controlled by appropriately selecting the control parameters.

4. Conclusions

The present paper provides a theoretical basis of the vibration control strategy based on the time-delayed acceleration feedback. The control force is synthesized by an infinite, weighted sum of the acceleration of the vibrating system measured at equal time interval in the past. Because the control signal can be alternatively expressed as a recursive sum of the acceleration and the control signal with a specific time-delay, the practical implementation of the controller does not pose any serious problem. The controller can be implemented using both analog and digital electronics.

Efficacy of the proposed control strategy in mitigating the resonant and low-frequency non-resonant vibrations of a single-degree-of-freedom linear undamped oscillator is first discussed. Ordinarily, vibrations cannot be controlled uniformly over the entire low-frequency and the resonant frequency band. Resonant vibrations can be controlled by decreasing the time-delay and this is generally achieved at the cost of increased low-frequency vibrations. However, for some choices of the control parameters (when the recursive parameter is set to unity), the entire low-frequency band including the resonance band can be uniformly controlled by decreasing the time-delay. Further improvement is possible by increasing the gain within the stability limit. The frequency-response characteristics of the controlled system are explained using the concept of an equivalent damping and the natural frequency. An approximate analysis shows that the damping factor can be maximized by increasing the value of the recursive parameter. It is also possible to generate a very large amount of damping by appropriately selecting the recursive parameter and the time-delay. The asymptotic property of the damping factor shows an interesting behavior in the small delay limit. When the recursive parameter is less than unity, the damping factor varies proportional to the time-delay in the small delay limit. However, this behavior changes drastically when the recursive parameter is chosen as unity. Under these circumstances, the effective damping is inversely related to the time-delay. Methods of optimizing the system response for the both forced and transient vibrations are also discussed.

The success of the control at lower values of the delay has an immense practical implication because the amount of data needs to be stored in the memory becomes less. However, there is also an increased chance of deterioration of the performance because of the latency period of the control.

The efficacy of the control strategy in controlling the primary and the 1/3 subharmonic resonances of a Duffing oscillator is also discussed. Using multiple time-scale analysis, it is shown that the primary resonance response can be controlled to a great extent and the occurrence of the jump can be delayed up to a large strength of the excitation. The 1/3 subharmonic resonance can either be completely eliminated or its amplitude can be reduced by appropriately selecting the control parameters.

The theoretical analysis presented here has established the efficacy of the proposed method in controlling the linear and nonlinear vibrations. However, the present study considers only a single mode of vibration. Future research should explore the efficacy of the method in simultaneously controlling the multiple modes of vibration and the influence of the control on the higher uncontrolled modes of vibration. Efficacies of the nonlinear recursive feedback control should be a subject of the future research. Experimental validations of the proposed control strategies will also be needed.

Acknowledgment

The author thanks the anonymous reviewers of the article for making valuable comments, which have triggered important questions that are to be addressed in future research.

Appendix A

It is to show that for $R<1$, the effective damping factor $\xi \propto \tau$ in the small delay limit. It is shown in Section 2.5 that the real poles of the system are obtained by solving the following nonlinear algebraic equation (same as Eq. (34)):

$$1 + x^2 - e^{-x\tau}\left[R + x^2(R + k_c)\right] = 0 \tag{A.1}$$

Eq. (A.1) is rewritten in the following form:

$$x = -\frac{1}{\tau}L(x), \tag{A.2}$$

where

$$L(x) = \ln\left(\frac{1 + x^2}{R + (R + k_c)x^2}\right).$$

It is easy to see that for $R + k_c > 0$, $\lim_{x\to\infty} L(x) = \ln(1/R + k_c)$ and $\lim_{x\to 0} L(x) = \ln(1/R)$. Thus from Eq. (A.2), it may be inferred that $x \propto (1/\tau) \Rightarrow x = (-k/\tau)$, where k is the constant of proportionality. Now comparing the denominators of Eqs. (26) and (27) and equating the coefficients of equal powers of s, the following relations are obtained:

$$2\xi\omega_n + \frac{k}{\tau} = \frac{2(1 - R)}{\tau(1 + R)}, \tag{A.3}$$

$$k\omega_n^2 = 2(1 - R) \tag{A.4}$$

and

$$\omega_n^2 + \frac{2k\xi\omega_n}{\tau} = \frac{1 + R}{1 + R + k_c}. \tag{A.5}$$

Eq. (A.4) reveals that in the small delay limit, the natural frequency is more or less independent of the time-delay. From Eq. (A.3), it is observed that k is also independent of τ in the small delay limit. Thus, it is clear from Eq. (A.5) that in the small delay limit, $\xi \propto \tau$.

References

[1] A.K. Agrawal, J.N. Yang, Compensation of time-delay for control of civil engineering structures, *Earthquake Engineering and Structural Dynamics* 29 (2000) 37–62.

[2] K. Gu, S. Niculescu, Survey on recent results in the stability and control of time-delay systems, *Journal of Dynamic Systems, Measurement and Control—Transactions of the ASME* 125 (2003) 158–165.

[3] N. Olgac, B.T. Holm-Hansen, A novel active vibration absorption technique: delayed resonator, *Journal of Sound and Vibration* 176 (1994) 93–104.

[4] N. Jalili, N. Olgac, Multiple identical delayed-resonator vibration absorbers for multi-degree-of freedom mechanical structures, *Journal of Dynamic Systems, Measurement, and Control—Transactions of the ASME* 122 (2000) 314–322.

[5] F.E. Udwadia, Noncollocated point control of nondispersive distributed-parameter systems using time-delays, *Applied Mathematics and Computation* 42 (1) (1991) 23–63.

[6] F.E. Udwadia, Noncollocated time-delayed control of continuous systems with tip-inertias, *Applied Mathematics and Computation* 47 (1992) 47–75.

[7] F.E. Udwadia, R. Kumar, Time-delayed control of classically damped structural systems, *International Journal of Control* 60 (1994) 687–713.

[8] F.E. Udwadia, H. von Bremen, R. Kumar, M. Hosseini, Time-delayed control of structures, *Earthquake Engineering and Structural Dynamics* 32 (2003) 495–535.

[9] F.E. Udwadia, H. von Bremen, P. Phohomsiri, Time-delayed control design for active control of structures: principles and application, *Structural Control Health Monitoring* 12 (3) (2005).

[10] P. Phohomsiri, F.E. Udwadia, H.F. von Bremen, Time-delayed positive velocity feedback control design for active control of structures, *Journal of Engineering Mechanics—Transactions of the ASCE* (2006) 690–703.

[11] H. Hu, E.H. Dowell, L.N. Virgin, Resonances of a harmonically forced Duffing oscillator with time-delay state feedback, *Nonlinear Dynamics* 15 (1998) 311–327.

[12] A. Maccari, Vibration control for the primary resonance of a cantilever beam by a time-delay state feedback, *Journal of Sound and Vibration* 259 (2003) 241–251.
[13] A. Maccari, Vibration control for the primary resonance of the van der Pol oscillator by a time-delay state feedback, *International Journal of Nonlinear Mechanics* 38 (2003) 123–131.
[14] A. Maccari, Vibration control for parametrically excited Liénard systems, *International Journal of Non-Linear Mechanics* 41 (2006) 146–155.
[15] F.M. Atay, Van der Pol's oscillator under delayed feedback, *Journal of Sound and Vibration* 218 (1998) 333–339.
[16] S. Chatterjee, Time-delayed feedback control of friction induced instabilities, *International Journal of Non-Linear Mechanics* 42 (9) (2007) 1127–1143.
[17] Z.N. Masoud, A.H. Nayfeh, N.A. Nayfeh, Sway reduction on quay-side container cranes using delayed feedback controller: simulations and experiments, *Journal of Vibration and Control* 11 (2005) 1103–1122.
[18] A. Preumont, N. Loix, D. Malaise, O. Lecrenier, Active damping of optical test benches with acceleration feedback, *Machine Vibration* 2 (1993) 119–124.
[19] S.J. Dyke, Acceleration Feedback Control Strategies for Active and Semi-active Control Systems: Modeling, Algorithm Development, and Experimental Verification, PhD Dissertation, Department of Civil Engineering and Geological Sciences, Notre Dame, Indiana, 1996.
[20] J.E.S. Socolar, D.W. Sukow, D.J. Gauthier, Stabilizing unstable periodic orbits in fast dynamical systems, *Physical Review E* 50 (1994) 3245–3248.
[21] A. Chang, J.C. Bienfang, G.M. Hall, J.R. Gardner, D.J. Gauthier, Stabilizing unstable steady states using extended time-delay autosynchronization, *CHAOS* 8 (4) (1998) 782–790.